



Numerical Simulation and Analysis of Residual Stress in B91 Steel Deposition Using Wire Arc Additive Manufacturing

Atilla Savaş^{*}

Mechanical Engineering Department, Piri Reis University, 34940 Istanbul, Turkey

^{*} Correspondence: Atilla Savaş (asavas@pirireis.edu.tr)**Received:** 04-28-2024**Revised:** 06-15-2024**Accepted:** 06-22-2024

Citation: A. Savaş, "Numerical simulation and analysis of residual stress in B91 steel deposition using Wire Arc Additive Manufacturing," *Precis. Mech. Digit. Fabr.*, vol. 1, no. 2, pp. 102–110, 2024. <https://doi.org/10.56578/pmdf010205>.



© 2024 by the author(s). Published by Acadlore Publishing Services Limited, Hong Kong. This article is available for free download and can be reused and cited, provided that the original published version is credited, under the CC BY 4.0 license.

Abstract: A numerical model of a Gas Metal Arc Welding (GMAW)-based Wire Arc Additive Manufacturing (WAAM) process was developed using the Abaqus software, with validation performed against experimental data from existing literature. The model was employed to investigate the influence of heat input and cooling time on residual stress distribution, with particular focus on longitudinal residual stress. Minimal effect was observed with increasing heat input, whereas cooling time significantly affected stress distribution. The impact of unclamping was also examined. It was determined that for heat inputs of 4000 W and 4500 W, longitudinal residual stress decreased by approximately 10% after unclamping. In contrast, for a heat input of 5000 W, longitudinal residual stress increased by 12% following unclamping. Residual stress was found to accumulate predominantly at the interface between the substrate and the deposition wall. This study provides critical insights into the thermal and mechanical behavior of WAAM processes, contributing to a deeper understanding of stress management and control in additive manufacturing of B91 steel.

Keywords: Wire Arc Additive Manufacturing (WAAM); Gas Metal Arc Welding (GMAW); Residual stress; Numerical simulation; Finite element method

1 Introduction

The drive for cost reduction in shipbuilding leads to the development of new ways for producing complex shapes. WAAM is a viable option for this purpose. Taşdemir and Nohut [1] stated that WAAM can manufacture massive and intricate ship parts. Residual stress and deformation may arise while manufacturing these parts. They may impede the usage of these components. Many researchers studied the temperature and residual stress distributions following a WAAM process. Mokrov et al. [2] investigated the modification of a double ellipsoidal heat source for the GMAW method. Israr et al. [3] devised a variable-power WAAM approach to reduce heat accumulation between welding passes. Consequently, the power consumption was also diminished.

Ding et al. [4] constructed an efficient Finite Element Model to simulate the temperature and stress distributions following the WAAM procedure. The computationally efficient model employed the Eulerian steady-state technique rather than the Lagrangian transient approach. This strategy is suitable for long welding seams because it can produce poor results at the start and end of the welding seam. As a result, it is not suitable for welding short seams. Denlinger et al. [5] developed an Electron Beam Welding (EBW)-based WAAM simulation. They accurately computed the distortion using their thermomechanical model.

Montevecchi et al. [6] developed a new moving heat source model as an alternative to the Goldak double-ellipsoidal heat source. Their model anticipated the temperatures and distortions really precisely. Graf et al. [7] studied the CMT-based WAAM technique for a variety of materials. Their thermomechanical models were compared to actual tests. They used the MSC Marc software to predict the circular material deposition on a substrate. Oyama et al. [8] explored heat source management in the WAAM method.

Jimenez et al.'s [9] study used an A36 substrate and a B91 filler material. They also used the phase transition phenomena to calculate the temperature and stress distributions following the WAAM procedure.

Saadatmand and Talemi [10] used A36 mild steel to replicate the thermal behavior of a plate following the WAAM process. They experimented with different heat inputs and preheating temperatures to see how these affected the

thermal cycle. Bauer et al. [11] investigated a CMT-based WAAM technique. Their investigation includes simulations generated by both commercial and open-source code. They had good outcomes compared to the experiments. Kovšca et al. [12] used the WAAM technique to deposit material in a circular pattern. They used the Simulia software to simulate the thermomechanical behavior of the generated item. The sequential thermomechanical analysis produced an excellent agreement between measured and modeled temperatures.

Ahmad et al. [13] used two different heat sources, Goldak double ellipsoidal and Goldak rectangular, to imitate the heat input from the WAAM process. Bonifaz and Palomeque evaluated the mechanical properties of a welded plate using a WAAM technique [14]. They concluded that increasing the welding speed causes an increase in residual stress. Huang et al. [15] modeled an Abaqus WAAM using in-house programs. They were able to significantly reduce computing time using their algorithms. Tangestani et al. [16] developed a model to predict stress distribution following the WAAM, forging, and rolling operations. They concluded that the residual stress in the pinch rolling process was dependent on the rolling direction.

Savaş [17] investigated welding procedures using Gas Tungsten Arc Welding (GTAW) and GMAW [18]. These publications looked at hard-facing processes that used GTAW and GMAW technologies. Sun et al. [19] studied Wire Arc Additive Manufacturing of aluminum parts. They proposed strategies for reducing residual stresses following a WAAM process.

Abusalma et al. [20] investigated a GMAW-based WAAM technique. Two distinct materials were deposited on a plate, and the effect of torch travel speed and cooling time on the layers was investigated. The interlayer cooling time has the greatest influence on residual tensions. The current work studied the effect of cooling time on longitudinal and build direction stress distributions.

Ghanavati et al.'s [21] work dealt with laser deposition of the Directed Energy Deposition method. Their work revealed that the residual stresses accumulate at the structure substrate interface. Sampaio et al. [22] made a review of the WAAM process studies. One of their findings is that after unclamping the structure, residual stress becomes both compressive and tensile.

In this study, we investigated the effect of heat input and waiting time between layers (cooling time) on residual stress. A GMAW-based WAAM process was designed. A computationally efficient half-domain was created, with fine mesh in and near the welding layers and coarse mesh in other sections chosen to efficiently handle the problem. The impact of unclamping the supports after welding was also explored in this study. The unclamping effect on the residual stress is an important part of this work. The validation of the numerical solution was performed according to literature [9].

2 Methodology

The Abaqus software was chosen for the simplicity of investigating the residual stress change after unclamping. In some other software, the unclamping effect could not be calculated directly from the initial solution. The geometrical domain and the material properties are given in the succeeding paragraphs.

Figure 1 demonstrates the partitioned and meshed problem domains. The calculation domain was partitioned so that it would mesh tightly on the symmetry plane and loosely on regions away from the centerline. The length is 100 mm, the breadth 50 mm, and the thickness 10 mm. Ten layers of 1 mm thick B91 metal are placed along the symmetry line. The layers are four millimeters wide. The substrate material is A36 steel. Figure 2 shows the temperature-dependent thermal characteristics of A36 and B91 steels. The density of each steel is 7800 kg/m^3 . The melting points for A36 and B91 steels are 1425 and 1420 centigrade degrees.

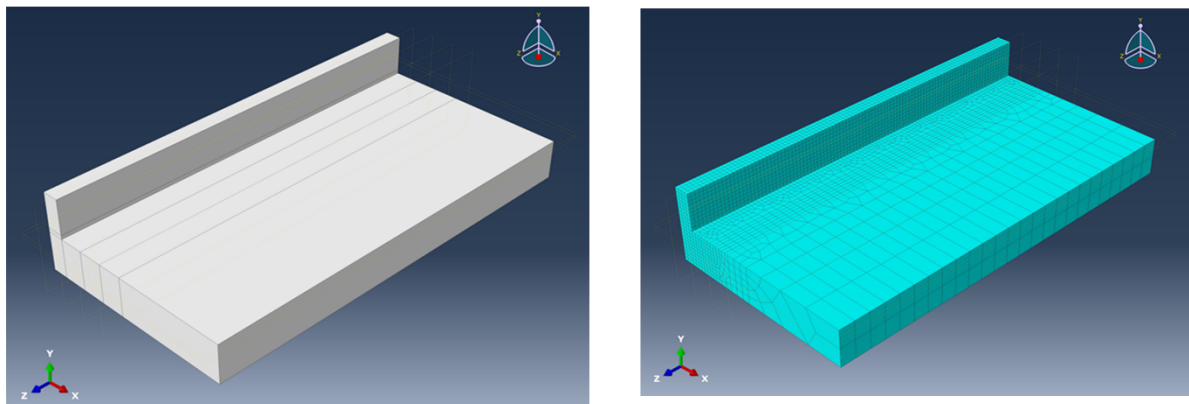


Figure 1. The partitioned and the enmeshed domains

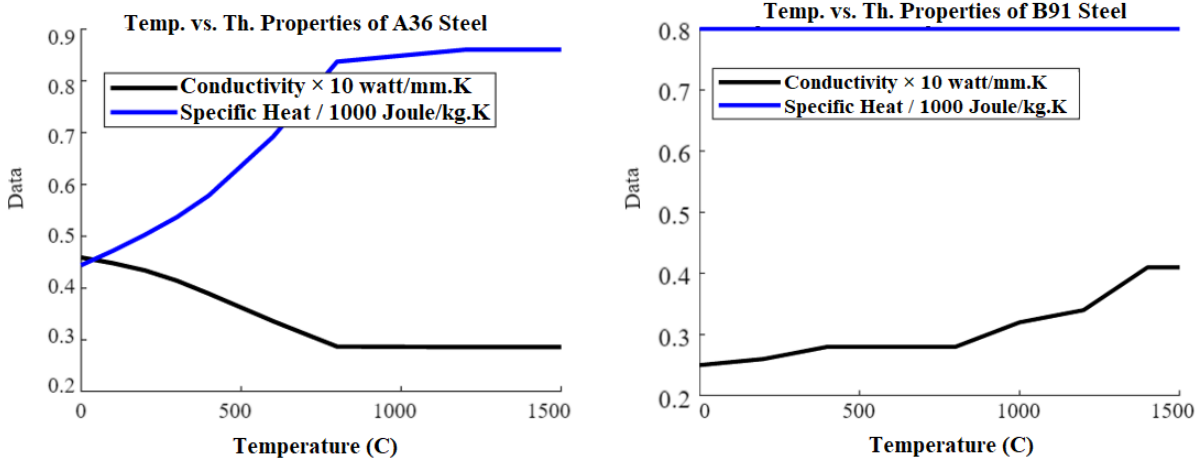


Figure 2. Thermal properties of A36 and B91 [23, 24]

2.1 WAAM Simulation

The heat input is the most significant aspect of the model. The two-part Goldak double ellipsoidal moving heat source model is provided below [18, 25]. The Goldak constants are depicted in Figure 3.

$$q_f(x, y, z) = \frac{6\sqrt{3}(f_f Q)}{abc_f \pi \sqrt{\pi}} \exp\left(-\frac{3x^2}{a^2} - \frac{3y^2}{b^2} - \frac{3z^2}{c_f^2}\right) \quad (1)$$

$$q_r(x, y, z) = \frac{6\sqrt{3}(f_r Q)}{abc_r \pi \sqrt{\pi}} \exp\left(-\frac{3x^2}{a^2} - \frac{3y^2}{b^2} - \frac{3z^2}{c_r^2}\right) \quad (2)$$

The values of the constants that are used in Eqs. (1) and (2) are presented in Table 1. Q value is given as 4000 watts. Q value is calculated as the product of voltage, amperage, and efficiency (η) of the welding process. These values are tabulated in the same table.

Table 1. Goldak constants and heat input

a	4 mm	V	28.5 V
b	4 mm	A	200, 225, 250 A
c _f	3 mm	η	0.7
c _r	6 mm	Q	4000, 4500, 5000 W
f _f	0.6	Cooling time	70, 150 s
f _r	1.4		

The transient temperature distribution was calculated according to the equation below:

$$\rho C \frac{\partial T}{\partial t}(x, y, z, t) = -\nabla \cdot (-k \nabla T) + Q(x, y, z, t) \quad (3)$$

Abaqus software was utilized to obtain the temperature distribution and the temperature history. The temperature distribution for the first, fifth, and tenth layers is given in Figure 4.

The temperature increase can be seen from the figure even though a sufficient amount of cooling time has been used. This cooling time parameter is going to be changed in the succeeding parts.

The convective heat transfer coefficient and radiation emissivity were taken as 10 W/(m² °C) and 0.4, respectively. The lower surface of the substrate has a convective heat transfer coefficient of 70 W/(m² °C) to consider the thermal contact conductance. The ambient temperature was taken as 25°C. The outer corners of the plates are chosen as fixed supports. The validation was performed according to Jimenez et al.'s work [9].

After the temperature history was obtained, sequentially coupled nonlinear stress analysis was performed using the temperature-dependent mechanical material properties in Figure 5, and Table 2 and Table 3. The computation time for the thermal part is one hour, and that of the structural part is about five hours. An Intel(R) Core(TM) i7 CPU @ 2.60GHz and 16 GB RAM computer was used.

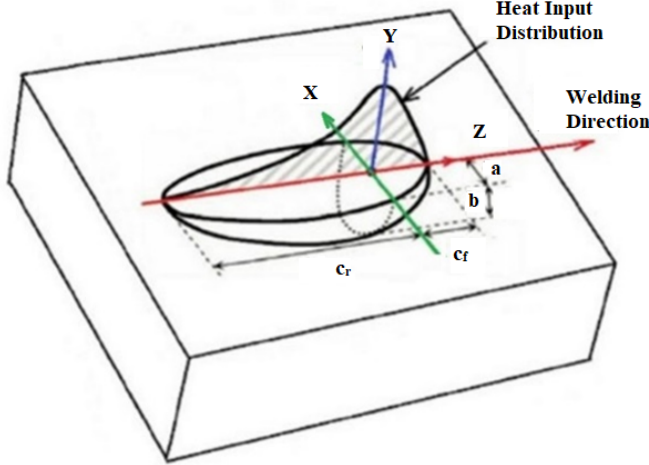


Figure 3. Goldak heat input constants [18, 25]

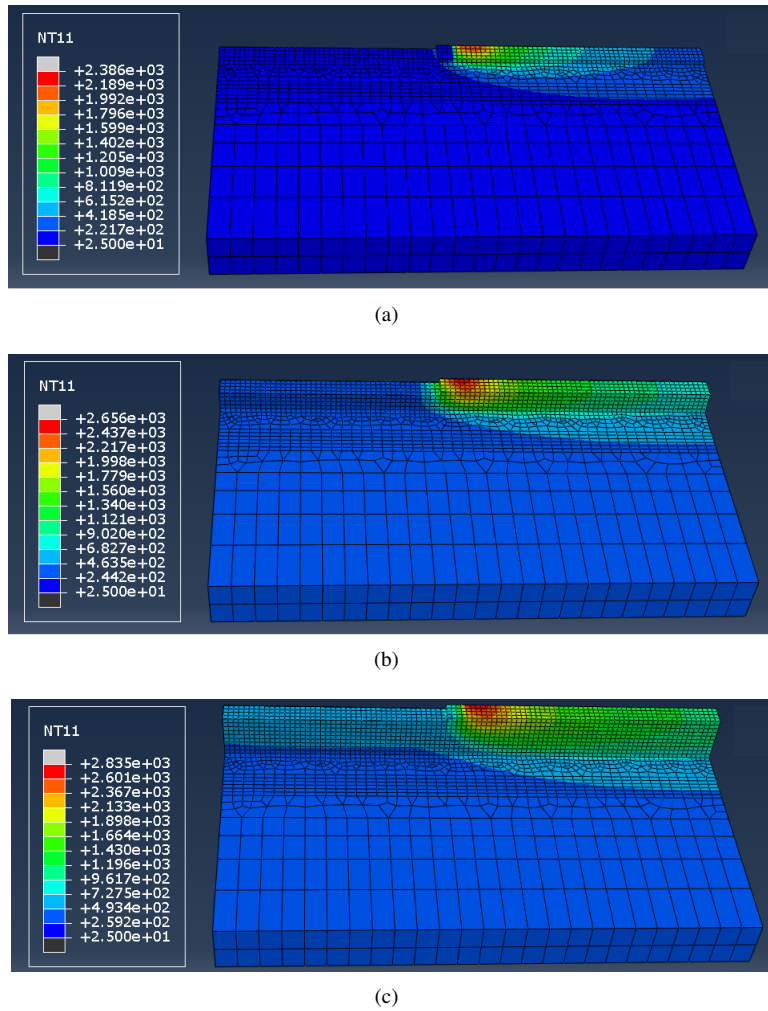


Figure 4. The temperature distribution for the first, fifth, and tenth layer deposition

After the temperature history has been calculated, the temperature load is applied to the static structural module of Abaqus. The strains are calculated according to the following formula:

$$\varepsilon_{total} = \varepsilon_{elastic} + \varepsilon_{plastic} + \varepsilon_{thermal} \quad (4)$$

After the validation according to the reference [9], the heat input was increased to 4500 W and 5000 W. Another

parameter to change was the cooling time between the layers. This value was changed from 70 to 150 seconds. The influence of heat input increase and increase in the cooling time has been studied.

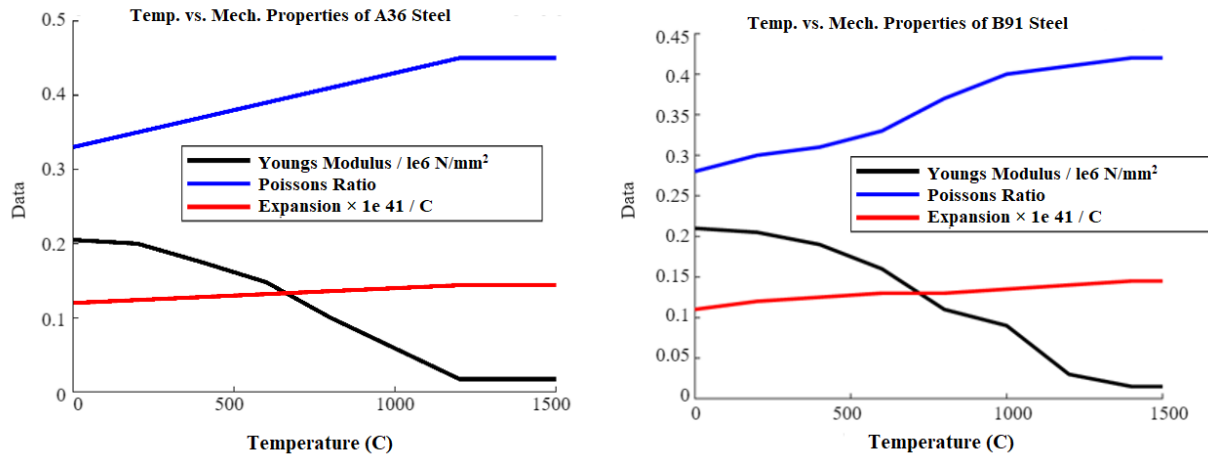


Figure 5. Mechanical properties of A36 and B91 steels [23, 24]

Table 2. Plastic behaviour of A36 steel [26]

Yield Stress (MPa)	Plastic Strain	Temperature °C
250	0	20
340	0.05	20
200	0	350
414	0.035	350
150	0	400
345	0.02	400
100	0	450
345	0.045	450
100	0	500
165	0.015	500
100	0	800
165	0.015	800
100	0	1500
165	0.015	1500

Table 3. Plastic behaviour of B91 steel [24]

Yield Stress (MPa)	Plastic Strain	Temperature °C
550	0	0
561	0.01	0
500	0	200
510	0.01	200
470	0	400
479	0.01	400
310	0	600
313	0.01	600
150	0	800
152	0.01	800
100	0	1000
101	0.01	1000
50	0	1200
51	0.01	1200

The validation heat input is 4000 Watts, and the welding speed is 4 mm/s. While comparing the temperatures, one can see a slight difference up to 400 seconds (Figure 6). This may be caused by the smaller welding speeds for the first two layers in the experiment. To make the computation easier, the welding speed was taken as constant (4 mm/s) for all of the layers. In our model, the equivalent stress values for the points P1 and P2 are 45 and 180 MPa, while the experimental stresses are 52 and 216 MPa [9]. Therefore, the temperature history and the stress distribution can be used to calculate other stress values.

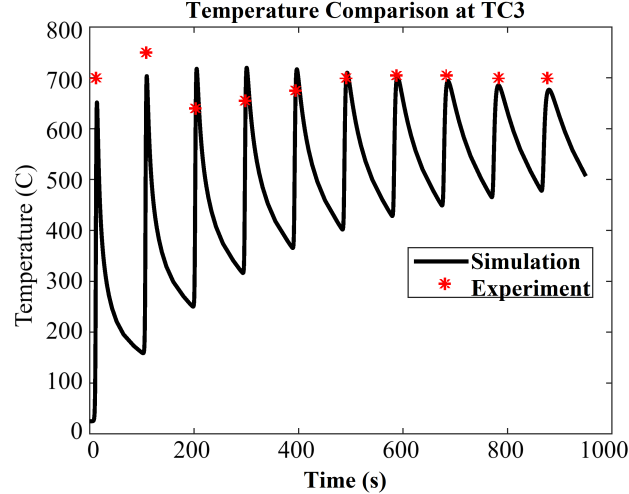


Figure 6. Temperature history comparison [9]

3 Results

The residual stress on two paths (Figure 7) on the substrate has been calculated and compared with each other. The heat input was selected as 4000, 4500, and 5000 Watts, and the cooling time between the layers was chosen as 70 and 150 seconds (Figure 8). The influence of heat input increase is negligible, whereas the influence of cooling time between layers is very significant. When one looks at Figure 8, one can easily conclude that the cooling time should be so arranged that sufficient cooling is performed and it should not be increased beyond that limit. To be on the safe side, several cooling times should be tried, and the optimum cooling time should be selected.

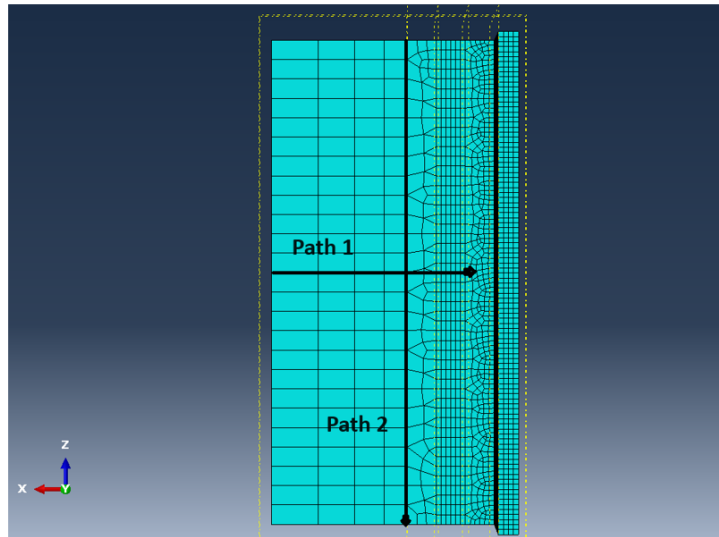


Figure 7. Path configuration for residual stress calculation

The important thing in Figure 8 is that when you increase the cooling time, you can get increased residual stress. The cooling time is the most important parameter in our calculations. The heat accumulation after the layers exceeds the heat loss due to convection and radiation.

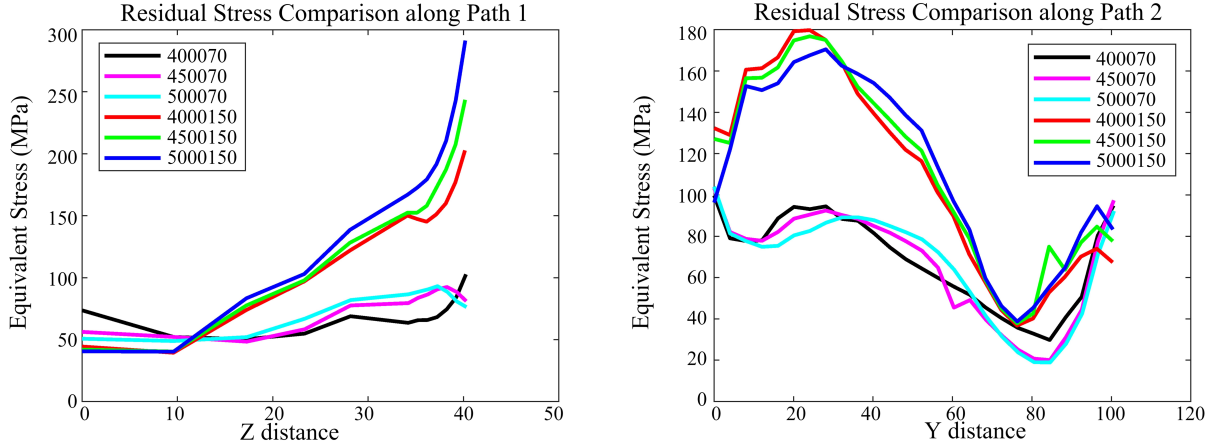


Figure 8. Residual stress comparison for Path 1 and Path 2

Note: 4000 corresponds to 4000 Watts and 70 corresponds to 70 seconds cooling between the layers. The other legend items can be deducted from the previous explanation.

The influence of unclamping in the z-direction (which is the most significant one) is presented in subgraphs (a)-(f) of Figure 9. S33 stands for the stress in the longitudinal direction.

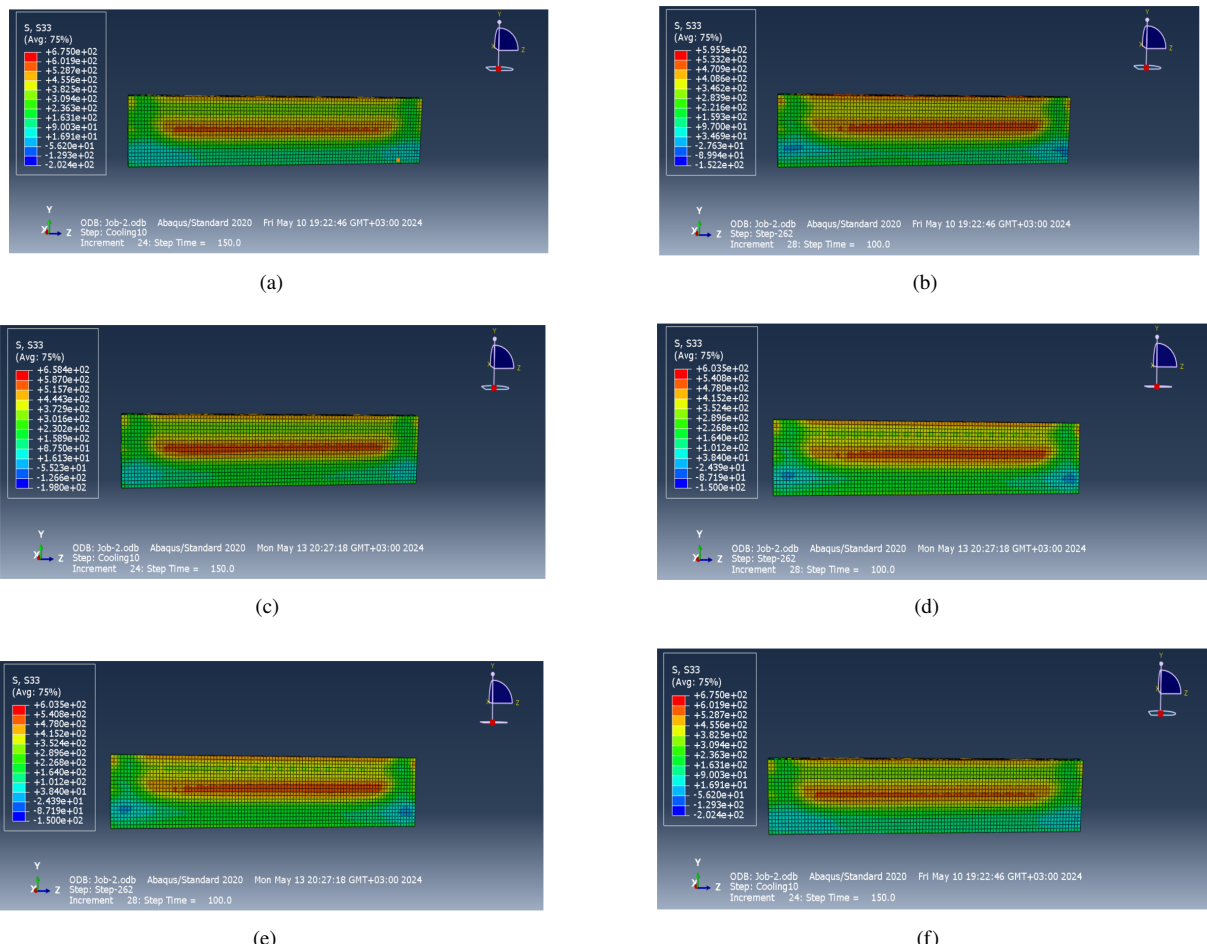


Figure 9. Residual stresses in longitudinal direction 4000 W(a,b) and 4500 W (c,d), 5000 W (e,f)

Note: The subgraph (a) of Figure 9 shows the stress after 150 seconds of cooling, the subgraph (b) of Figure 9 shows the stress 100 seconds after unclamping (Seen from the symmetry plane).

4 Discussion

In the longitudinal direction (z-axis), which has the most significant stress changes after the unclamping, with a small amount of heat input (i.e., 4000 and 4500 Watts), the stress relaxation of 8 to 12 percent has been observed. On the other hand, 5000 Watt heat input causes a stress increase of 12 percent after unclamping. One more important finding in these figures is that the residual stress accumulation is located on the substrate deposition wall interface.

5 Conclusions

An efficient model of the GMAW-based WAAM process has been prepared. The computation time was diminished by using a smart meshing technique. The cooling time between the layers has a very prominent effect on the residual stress. The amount of cooling time should be arranged so that the cooling effect would prevent heat accumulation and it should not increase the substrate stresses. The influence of heat input increase caused stress relaxation after unclamping for 4000 and 4500 Watts (8 to 12 percent). The unclamping with 5000 Watts heat input caused stress accumulation of 12 percent. Ghanavati et al.'s work [21] and our work have given similar results that the residual stress accumulation is located on the substrate and structure interface. Further research can be done by trying several cooling times, and then one can choose the optimum cooling time before performing a lot of experiments.

Data Availability

The data used to support the research findings are available from the corresponding author upon request.

Conflicts of Interest

The authors declare no conflict of interest.

References

- [1] A. Taşdemir and S. Nohut, "An overview of wire arc additive manufacturing (WAAM) in shipbuilding industry," *Ships Offshore Struct.*, vol. 16, no. 7, pp. 797–814, 2021. <https://doi.org/10.1080/17445302.2020.1786232>
- [2] O. Mokrov, M. Simon, A. Schiebahn, and U. Reisgen, "A fine modification of the double ellipsoid heat source," *Math. Model. Weld Phenom.*, vol. 12, pp. 39–50, 2019. <https://doi.org/10.3217/978-3-85125-615-4-04>
- [3] R. Israr, J. Buhl, and M. Bambach, "A study on power-controlled wire-arc additive manufacturing using a data-driven surrogate model," *Int. J. Adv. Manuf. Technol.*, vol. 117, pp. 2133–2147, 2021. <https://doi.org/10.1007/s00170-021-07358-y>
- [4] J. Ding, P. Colegrave, J. Mehnert, S. Williams, F. Wang, and P. S. S. Almeida, "A computationally efficient finite element model of wire and arc additive manufacture," *Int. J. Adv. Manuf. Technol.*, vol. 70, pp. 227–236, 2014. <https://doi.org/10.1007/s00170-013-5261-x>
- [5] E. R. Denlinger, J. C. Heigel, and P. Michaleris, "Residual stress and distortion modeling of electron beam direct manufacturing Ti-6Al-4V," *Proc. Inst. Mech. Eng. B: J. Eng. Manuf.*, vol. 229, no. 10, pp. 1803–1813, 2015. <https://doi.org/10.1177/0954405414539494>
- [6] F. Montevercchi, G. Venturini, A. Scippa, and G. Campatelli, "Finite element modelling of wire-arc-additive-manufacturing process," *Procedia CIRP*, vol. 55, pp. 109–114, 2016. <https://doi.org/10.1016/j.procir.2016.08.024>
- [7] M. Graf, A. Hälsig, K. Höfer, B. Awiszus, and P. Mayr, "Thermo-mechanical modelling of wire-arc additive manufacturing (WAAM) of semi-finished products," *Metals*, vol. 8, no. 12, p. 1009, 2018. <https://doi.org/10.3390/met8121009>
- [8] K. Oyama, S. Diplas, M. M'hamdi, A. E. Gunnæs, and A. S. Azar, "Heat source management in wire-arc additive manufacturing process for Al-Mg and Al-Si alloys," *Addit. Manuf.*, vol. 26, pp. 180–192, 2019. <https://doi.org/10.1016/j.addma.2019.01.007>
- [9] X. Jimenez, W. Dong, S. Paul, M. A. Klecka, and A. C. To, "Residual stress modeling with phase transformation for wire arc additive manufacturing of B91 steel," *JOM*, vol. 72, pp. 4178–4186, 2020. <https://doi.org/10.1007/s11837-020-04424-w>
- [10] M. Saadatmand and R. Talemi, "Study on the thermal cycle of Wire Arc Additive Manufactured (WAAM) carbon steel wall using numerical simulation," *Frattura Ed Integrità Strutturale*, vol. 14, no. 52, pp. 98–104, 2020. <https://doi.org/10.3221/IGF-ESIS.52.08>
- [11] A. Bauer, R. Scharf, A. Hälsig, and B. Awiszus, "Numerical simulation and calibration of a single seam WAAM process with a commercial and an open source software," *J. Appl. Eng. Des. Simul.*, vol. 1, no. 1, pp. 25–31, 2021. <https://doi.org/10.24191/jaeds.v1i1.21>
- [12] D. Kovšca, B. Starman, A. Ščetinec, D. Klobčar, and N. Mole, "Advanced computational modelling of metallic wire-arc additive manufacturing," in *ESAFORM 2021 - 24th International Conference on Material Forming*, 2021, pp. 1–13. <http://doi.org/10.25518/esaform21.2340>

- [13] S. N. Ahmad, Y. H. P. Manurung, M. F. Mat, Z. Minggu, A. Jaffar, S. Pruller, and M. Leitner, “FEM simulation procedure for distortion and residual stress analysis of wire arc additive manufacturing,” *IOP Conf. Ser.: Mater. Sci. Eng.*, vol. 834, p. 012083, 2020. <https://doi.org/10.1088/1757-899X/834/1/012083>
- [14] E. A. Bonifaz and J. S. Palomeque, “A mechanical model in wire + Arc additive manufacturing process,” *Prog. Addit. Manuf.*, vol. 5, pp. 163–169, 2020. <https://doi.org/10.1007/s40964-020-00112-y>
- [15] H. Huang, N. S. Ma, J. Chen, Z. L. Feng, and H. Murakawa, “Toward large-scale simulation of residual stress and distortion in wire and arc additive manufacturing,” *Addit. Manuf.*, vol. 34, p. 101248, 2020. <https://doi.org/10.1016/j.addma.2020.101248>
- [16] R. Tangestani, G. H. Farrahi, M. Shishegar, B. P. Aghchehkandi, S. Ganguly, and A. Mehmanparast, “Effects of vertical and pinch rolling on residual stress distributions in wire and arc additively manufactured components,” *J. Mater. Eng. Perform.*, vol. 29, pp. 2073–2084, 2020. <https://doi.org/10.1007/s11665-020-04767-0>
- [17] A. Savaş, “Investigating the thermal and structural responses in hard-facing application with the GTAW process,” *J. Theor. Appl. Mech.*, vol. 59, no. 3, pp. 343–353, 2021. <https://doi.org/10.15632/jtam-pl/136210>
- [18] A. Savaş, “Selection of welding conditions for minimizing the residual stresses and deformations during hard-facing of mild steel,” *Brodogradnja*, vol. 72, no. 1, pp. 1–18, 2021. <https://doi.org/10.21278/brod72101>
- [19] J. Sun, J. Hensel, M. Köhler, and K. Dilger, “Residual stress in wire and arc additively manufactured aluminum components,” *J. Manuf. Process.*, vol. 65, pp. 97–111, 2021. <https://doi.org/10.1016/j.jmapro.2021.02.021>
- [20] H. Abusalma, H. Eisazadeh, F. Hejripour, J. Bunn, and D. K. Aidun, “Parametric study of residual stress formation in wire and arc additive manufacturing,” *J. Manuf. Process.*, vol. 75, pp. 863–876, 2022. <https://doi.org/10.1016/j.jmapro.2022.01.043>
- [21] R. Ghanavati, H. Naffakh-Moosavy, M. Moradi, E. Gadalińska, and A. Saboori, “Residual stresses and distortion in additively-manufactured SS316L-IN718 multi-material by laser-directed energy deposition: A validated numerical-statistical approach,” *J. Manuf. Process.*, vol. 108, pp. 292–309, 2023. <https://doi.org/10.1016/j.jmapro.2023.11.018>
- [22] R. F. V. Sampaio, J. P. M. Pragana, I. M. F. Bragança, C. M. A. Silva, C. V. Nielsen, and P. A. F. Martins, “Modelling of wire-arc additive manufacturing – A review,” *Adv. Ind. Manuf. Eng.*, vol. 6, p. 100121, 2023. <https://doi.org/10.1016/j.aime.2023.100121>
- [23] H. Eisazadeh, A. Achuthan, J. A. Goldak, and D. K. Aidun, “Effect of material properties and mechanical tensioning load on residual stress formation in GTA 304-A36 dissimilar weld,” *J. Mater. Process. Technol.*, vol. 222, pp. 344–355, 2015. <https://doi.org/10.1016/j.jmatprotex.2015.03.021>
- [24] A. H. Yaghi, T. H. Hyde, A. A. Becker, and W. Sun, “Numerical simulation of P91 pipe welding including the effects of solid-state phase transformation on residual stresses,” *Proc. Inst. Mech. Eng., Part L: J. Mater.: Des. Appl.*, vol. 221, no. 4, pp. 213–224, 2007. <https://doi.org/10.1243/14644207JMDA152>
- [25] J. Goldak, A. Chakravarti, and M. Bibby, “A new finite element model for welding heat sources,” *Metall. Trans. B*, vol. 15, pp. 299–305, 1984. <https://doi.org/10.1007/BF02667333>
- [26] B. A. Fields and R. J. Fields, “Elevated temperature deformation of structural steel prepared for American Iron and Steel Institute,” 1989. [https://www.govinfo.gov/content/pkg/GOV PUB-C13-1774d8ff4cb40bdffe3035200dcbbd07.pdf](https://www.govinfo.gov/content/pkg/GOV PUB-C13-1774d8ff4cb40bdffe3035200dcbbd07/pdf/GOV PUB-C13-1774d8ff4cb40bdffe3035200dcbbd07.pdf)